

An analytical effective excess charge density model to predict the streaming potential generated by unsaturated flow

Mariangeles Soldi^{1,*}, Damien Jougnot², Luis Guarracino^{1,3}

(1) Consejo Nacional de Investigaciones Científicas y Técnicas, Facultad de Ciencias Astronómicas y Geofísicas, Universidad Nacional de La Plata, La Plata, Argentina

(2) Sorbonne Université, CNRS, EPHE, UMR 7619 Metis, F-75005, Paris, France

(3) Facultad de Ciencias Naturales y Museo, Universidad Nacional de La Plata, La Plata, Argentina

(*)Corresponding author: msoldi@fcaglp.unlp.edu.ar

This paper has been accepted for publication by Geophysical Journal International:

Soldi, M., Jougnot, D., & Guarracino, L. (2019). An analytical effective excess charge density model to predict the streaming potential generated by unsaturated flow. *Geophysical Journal International*, 216(1), 380-394. DOI: 10.1093/gji/ggy391.

Abstract

The self-potential (SP) method is a passive geophysical method that relies on the measurement of naturally occurring electrical field. One of the contributions to the SP signal is the streaming potential, which is of particular interest in hydrogeophysics as it is directly related to both the water flow and porous medium properties. The streaming current is generated by the relative displacement of an excess of electrical charges located in the electrical double layer surrounding the minerals of the porous media. In this study, we develop a physically based analytical model to estimate the effective excess charge density dragged by the water flow under partially saturated conditions. The proposed model is based on the assumption that the porous media can be represented by a bundle of tortuous capillary tubes with a fractal pore size distribution. The excess charge that is effectively dragged by the water flow is estimated using a flux averaging approach. Under these hypotheses, this new model describes the effective excess charge density as a function of saturation and relative permeability while also depending on the chemical and interface properties, and on petrophysical parameters of the media. The expression of the model has an analytical single closed-form which is consistent with a previous model developed from a different approach. The performance of the proposed model is then tested against previous models and different sets of laboratory and field data from the literature. The predictions of the proposed model fits fairly well the experimental data and shows improvements to estimate the magnitude of the effective excess charge density over the previous models. A relationship between the effective excess charge density and permeability can also be derived from the proposed model, representing a generalization to unsaturated conditions of a widely used empirical relationship. This new model proposes a simple and efficient way to model the streaming current generation for partially saturated porous media.

Keywords: Hydrogeophysics – Electrical properties – Fractal and multifractals – Permeability and porosity

1 Introduction

The self-potential (SP) method has gained a strong interest in reservoir and environmental studies due its sensitivity to water flow. Among many other applications of SP, one can mention its use to monitor water flow in the subsurface [e.g., Doussan et al., 2002, Darnet and Marquis, 2004, Jardani et al., 2007, Linde et al., 2011, Jougnot et al., 2015], geothermal systems [e.g., Corwin and Hoover, 1979, Revil et al., 1999b], oil and gas reservoirs [e.g., Saunders et al., 2006], and CO₂ sequestration [e.g., Moore et al., 2004, Büsing et al., 2017]. Although SP signals are relatively easy to measure, the recorded SP signals are a superposition of different contributions related to redox, diffusion and electrokinetic processes [for more details, see Revil and Jardani, 2013].

In the present work, we focus on the electrokinetic (EK) contribution to the total SP signal which is directly linked to water flow in porous media and is often referred to as streaming potential. Mineral surfaces are generally electrically charged, creating an electrical double layer (EDL) in the surrounding pore water (see Fig. 1a). The EDL contains an excess of charge distributed in two layers that counterbalances the mineral one [e.g., Hunter, 1981, Revil and Cerepi, 2004]: the Stern and the diffuse layer. When the water flows through the pore (Fig. 1c), the excess charge located in the diffuse layer (Fig. 1b) is dragged, which leads to a streaming current generation and a resulting electrical potential distribution. This EK phenomenon has been studied experimentally and theoretically for more than a century [e.g., Smoluchowski, 1903]. While the generation of the streaming potential has been well studied and modeled under saturated conditions [e.g., Jardani et al., 2007, Revil and Jardani, 2013, Guarracino and Jougnot, 2018], its generation under partially saturated conditions is still under discussion in the community and no consensus has been achieved regarding how to best model it.

Two main approaches can be used to model the streaming current generation under partially saturated conditions: (1) the Helmholtz-Smoluchowski coupling coefficient (or a variation of it to include the electrical surface conductivity) and (2) the excess charge that is effectively dragged in by the water. The streaming potential coupling coefficient has been defined to relate an electrical potential difference (i.e., the electrical field) and a hydraulic pressure difference (i.e., the groundwater flow). The first approach is therefore focused on the evolution of this parameter with varying water saturation [e.g., Guichet et al., 2003, Darnet and Marquis, 2004, Revil and Cerepi, 2004, Jackson, 2010, Vinogradov and Jackson, 2011, Allègre et al., 2015, Fiorentino et al., 2016]. The second approach results from a variable change where the coupling parameter is the excess charge that is effectively dragged by the water in the pore space [e.g., Linde et al., 2007, Revil et al., 2007, Jougnot et al., 2012, 2015]. This approach allows the decomposition of the streaming potential coupling coefficient in three components: the relative permeability, the electrical conductivity, and the effective excess charge density. Each of them varies with saturation and can be determined independently. The fact that these components behave differently with saturation and strongly depend on the soil texture is a likely explanation of why the behavior of the streaming potential coupling coefficient cannot be expressed in general [see discussion in Jougnot et al., 2012]. While the variation of the relative permeability and the electrical conductivity under variably saturated conditions have been the subject of many works during the last decades, the variation of the effective excess charge is still largely understudied [e.g., Revil et al., 2007, Jougnot et al., 2012, 2015, Zhang et al., 2017].

In this general context, the aim of our work is to develop a model following the excess charge approach that explicitly considers the dependence of the different parameters with saturation and the chemistry of the pore water.

Pore space in real porous media can be complex (e.g., the pores are three dimensional, some of them can be connected and have different geometrical shapes). Capillary tube models are a simple representation of the real pore space that have been used to provide valuable insight into transport in porous media. Jackson [2008, 2010], Linde [2009], Jougnot et al. [2012, 2015], Thanh et al. [2017], and Guarracino and Jougnot [2018] have successfully used these models to study the streaming potential phenomenon. Fractal distributions of the capillary tubes has proven to be useful to characterize porous media when describing hydrological processes and hydraulic properties for different soil textures [e.g., Tyler and Wheatcraft, 1990, Yu et al., 2003, Ghanbarian-Alavijeh et al., 2011, Guarracino et al., 2014, Xu, 2015, Soldi et al., 2017, Thanh et al., 2017]. In this study, we derive an analytical model to determine the effective excess charge density under partially saturated conditions. On the one hand, effective saturation and relative permeability curves are estimated by up-scaling the hydraulic properties at the pore scale to a bundle of capillary tubes with a fractal pore-size distribution. On the other hand, the effective excess charge density in a single capillary tube is calculated from the radial distributions of excess charge and water velocity. Therefore, at macroscopic scale the effective excess charge density is then estimated using a flux-averaging technique. Combining these hydraulic and EK properties, a closed-form expression for the effective excess charge density is obtained as a function of effective saturation and relative permeability. The resulting expression also relies on intrinsic petrophysical properties (i.e., permeability, porosity, tortuosity) and chemical interface properties (i.e., ionic concentration, zeta potential, Debye length). The performance of the proposed model is tested against different sets of experimental data and previous models. In addition, a relationship between the effective excess charge density and permeability can be derived. It is also shown that the estimates of the effective excess charge density can be satisfactorily extrapolated from saturated to partially saturated conditions by introducing the ratio of the effective saturation and relative permeability of the media.

2 Streaming potential framework

In the present section we introduce the theory used to describe the streaming current. Our work is based on the framework of Revil et al. [2007] in which SP signals can be related to water velocity directly. It focuses on the excess charge approach proposed by Jougnot et al. [2012] that describes the generation of these currents as an excess charge effectively dragged by the water flow.

The SP response of a given source current density \mathbf{J}_s (A/m²) can be described by two equations [Sill, 1983]:

$$\mathbf{J} = \sigma \mathbf{E} + \mathbf{J}_s, \quad (1)$$

$$\nabla \cdot \mathbf{J} = 0, \quad (2)$$

where \mathbf{J} (A/m²) is the total current density, σ (S/m) the bulk electrical conductivity,

$\mathbf{E} = -\nabla\varphi$ (V/m) the electrical field being φ (V) the electrical potential. In the absence of external current (i.e., no current injection in the medium), Eqs. (1) and (2) can be combined to obtain:

$$\nabla \cdot (\sigma \nabla \varphi) = \nabla \cdot \mathbf{J}_s. \quad (3)$$

Since EK processes often dominates SP signals in hydrological applications, we consider the streaming current density \mathbf{J}_s^{EK} as the source of \mathbf{J}_s . This current density is directly related to the water flux which follows Darcy's law [Darcy, 1856] and can be expressed as \mathbf{u} (m/s):

$$\mathbf{u} = -\frac{k}{\eta_w} \nabla(p - \rho_w g z) = -K \nabla H \quad (4)$$

where k (m²) is the permeability, η_w (Pa s) the water dynamic viscosity, p (Pa) the water pressure, ρ_w (kg/m³) the water density, g (m/s²) the gravitational acceleration, $K = \frac{\rho_w g k}{\eta_w}$ (m/s) the hydraulic conductivity, and $H = \frac{p}{\rho_w g} - z$ (m) the hydraulic head.

Traditionally this source current density is defined with the hydraulic gradient through the streaming potential coupling coefficient C_{EK} (V/m) [Helmholtz, 1879, Smoluchowski, 1903]:

$$\mathbf{J}_s^{EK} = \sigma C_{EK} \nabla H, \quad (5)$$

with C_{EK} defined as:

$$C_{EK} = \left. \frac{\partial \varphi}{\partial H} \right|_{\mathbf{J}=\mathbf{0}}, \quad (6)$$

where this coefficient measures the sensitivity between the electrical potential and the variation of the hydraulic head of the water.

Based on simple analytical developments, Kormiltsev et al. [1998] and Revil and Leroy [2004] express the coupling coefficient as a function of the effective excess charge density. Following Revil and collaborators formalism, it yields:

$$C_{EK}^{sat} = -\frac{\hat{Q}_v^{sat} k}{\sigma^{sat} \eta_w}, \quad (7)$$

where \hat{Q}_v^{sat} (C/m³) is the excess charge density in the diffuse layer per pore water volume and σ^{sat} (S/m) the electrical conductivity of the medium at saturation. Equation (7) can be extended under partially water-saturated conditions as follows [e.g., Linde et al., 2007, Jackson, 2010]:

$$C_{EK}(S_w) = -\frac{\hat{Q}_v(S_w) k_{rel}(S_w) k}{\sigma(S_w) \eta_w}, \quad (8)$$

where k_{rel} is the relative permeability which is a dimensionless function of water saturation S_w and varies between 0 and 1, σ (S/m) the electrical conductivity of the media and \hat{Q}_v (C/m³) the excess charge density which are also functions of the water saturation. Several models from the literature can be used to describe the dependence of these petrophysical properties k_{rel} and σ with S_w . Two of the most widely used model to estimate k_{rel} are

Brooks and Corey [1964] and van Genuchten [1980], while Archie's second law (1942) and Waxman and Smits [1968] are commonly used to predict the electrical conductivity.

Note that \mathbf{J}_s^{EK} (Eq. 5) can be expressed using directly the effective excess charge density under partially saturated conditions and the flux velocity, it yields:

$$\mathbf{J}_s^{EK} = \hat{Q}_v(S_w)\mathbf{u} \quad (9)$$

In the following subsections the hydraulic and electrokinetic properties at microscale (for one single pore) and macroscale (representative elementary volume, REV) scale are presented.

2.1 Pore scale

2.1.1 Hydraulic properties

The porous medium is represented by a bundle of circular-tortuous capillary tubes. Each pore is conceptualized as a cylindrical tube of radius R (m), length l (m) and hydraulic tortuosity τ (dimensionless) which can be defined as the ratio l/L being L (m) the length of the REV at macroscale.

The volume of a single pore is then given by:

$$V_p(R) = \pi R^2 l, \quad (10)$$

and the average velocity in the capillary tube \bar{v} (m/s) can be obtained from the Poiseuille law, assuming laminar flow, as:

$$\bar{v}(R) = \frac{\rho_w g}{8\eta_w \tau} R^2 \frac{\Delta h}{L}, \quad (11)$$

where Δh (m) is the pressure head drop across the REV.

2.1.2 Electrokinetic properties

The electrokinetic behavior of a capillary is mainly determined by the previously derived $\bar{v}(R)$ and the chemical composition of the pore water. Then, we consider that each capillary tube is saturated by a binary symmetric 1:1 electrolyte with a ionic concentration C_w^0 (mol/L) (e.g., NaCl). Since the mineral's surface is generally electrically charged, there exists an excess of charge in the pore water in order to assure the electrical neutrality: the electrical double layer (EDL). It can be distinguished from the free electrolyte where there are no charges present (see Fig. 1). The EDL is composed by two layers, close to the capillary wall is where most of that excess charge is fixed in the Stern layer while the remaining part of it is distributed in the Gouy-Chapman layer (or diffuse layer, Fig. 1a,b). The interface between these two layers can be approximated by a plane of shear which separates the stationary and non-stationary fluid [Hunter, 1981]. This plane is characterized by an electrical potential called zeta potential ζ (V), which depends on ionic strength, temperature, pH, among other quantities [e.g., Revil et al., 1999a].

To study the electrokinetic properties, the Stern layer can be neglected since it is beyond the shear plane and the water flow [e.g., Leroy and Revil, 2004, Tournassat et al.,

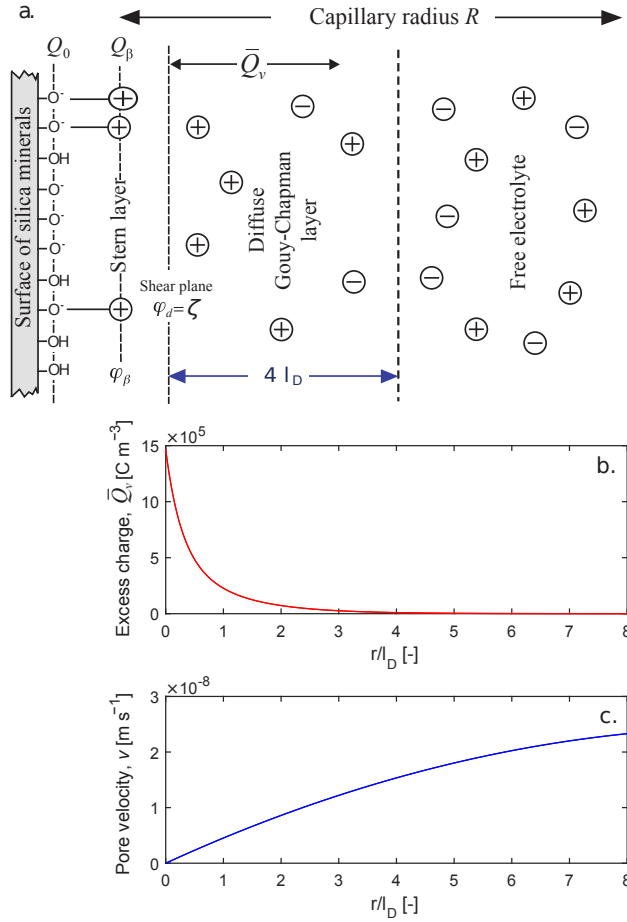


Figure 1: (a) Scheme of the electrical layers within a capillary tube of radius R . (b) and (c) distributions of the static excess charge and the pore water velocity as a function of the distance from the mineral surface in the capillary, respectively.

2009]. Therefore, we are interested in the Gouy-Chapman layer where the fluid is non-stationary, the thickness of this layer is given in terms of the Debye length l_D (m) which is defined as [Hunter, 1981]:

$$l_D = \sqrt{\frac{\epsilon k_B T}{2N_A C_w^0 e_0^2}} \quad (12)$$

where ϵ (F/m) is the pore water dielectric permittivity, k_B (J/K) the Boltzmann constant, T (K) the absolute temperature, N_A (1/mol) the Avogadro's number, C_w^0 the ionic concentration far from the mineral surface and e_0 (C) the elementary charge. The Gouy-Chapman layer's (i.e., diffuse layer) thickness is assumed to be four Debye lengths [Hunter, 1981]. Indeed, as it can be seen in Fig. 1, the excess charge distribution tends to zero as the distance to the mineral surface diminishes.

Recently, Guarracino and Jougnot [2018] developed a physically based analytical model to estimate the effective excess charge density dragged in the capillary by the water flow under saturated conditions (see Fig. 1b and c). Considering the thin double layer assumption (i.e., the thickness of the double layer is small compared to the pore

size, $l_D \ll R$), they found that the effective excess charge density carried by the water flow in a single tube of radius R is given by:

$$\hat{Q}_v^R = \frac{8N_A e_0 C_w^0}{(R/l_D)^2} \left[-\frac{2e_0\zeta}{k_B T} - \left(\frac{e_0\zeta}{3k_B T} \right)^3 \right]. \quad (13)$$

Note that according to Guarracino and Jougnot [2018], the above equation is valid for capillaries whose radii R are greater than $5l_D$. In Section 2.2.2, Eq. (13) is used to estimate \hat{Q}_v in a porous medium under partially saturated conditions.

2.2 REV scale

In order to derive the hydraulic and electrokinetic properties at macroscale we consider as representative elementary volume (REV) a cylinder of radius R_{REV} (m) and length L (m). The porous medium of the REV is conceptualized as an equivalent bundle of capillary tubes with a fractal pore size distribution and the pore structure is represented by the geometry described in the previous section with radii varying from a minimum pore radius R_{min} (m) to a maximum pore radius R_{max} (m).

The cumulative size-distribution of pores whose average radii are greater than or equal to R is assumed to obey the following fractal law [Tyler and Wheatcraft, 1990, Yu et al., 2003, Guarracino et al., 2014, Soldi et al., 2017, Guarracino and Jougnot, 2018]:

$$N(R) = \left(\frac{R_{REV}}{R} \right)^D \quad (14)$$

where D is the fractal dimension of pore size with $1 < D < 2$ and $0 < R_{min} \leq R \leq R_{max} < R_{REV}$. It is worth mentioning that D can be considered as a measure of the soil texture where the highest values of D are associated with the finest textured soils [Tyler and Wheatcraft, 1990]. Differentiating Eq. (14) with respect to R we obtain the number of pores whose radii are in the infinitesimal range R to $R + dR$:

$$dN(R) = -DR_{REV}^D R^{-D-1} dR \quad (15)$$

where the negative sign implies that the number of pores decreases with the increase of pore radius R .

The porosity of the REV can be computed from its definition as the quotient between the volume of pores and the volume of the REV which yields [Guarracino and Jougnot, 2018]:

$$\phi = \frac{\tau D}{R_{REV}^{2-D}(2-D)} (R_{max}^{2-D} - R_{min}^{2-D}). \quad (16)$$

The parameter τ can be defined for the entire model because the length of the pores is assumed to be independent of the capillary radius (i.e., τ is the same for all the capillaries).

2.2.1 Saturation and relative permeability curves

In this section, we consider the REV under partially saturated conditions. Then, the contribution to the water flow is given by the effective saturation S_e (dimensionless), defined by:

$$S_e = \frac{S_w - S_w^r}{1 - S_w^r}, \quad (17)$$

where S_w and S_w^r are the water saturation and residual water saturation, respectively.

In order to obtain the effective saturation curve, we consider that the REV is initially fully saturated and then drained when submitted to a pressure head h (m). For a straight capillary tube, we can relate a pore radius R_h (m) to h by the following equation [e.g., Jurin, 1717, Bear, 1998]:

$$h = \frac{2T_s \cos(\beta)}{\rho_w g R_h}, \quad (18)$$

where T_s (N/m) is the surface tension of the water and β , the contact angle. A capillary becomes fully desaturated if its radius R is greater than the radius R_h given by Eq. (18). Then, it is reasonable to assume that pores with radii R between R_{min} and R_h will remain fully saturated. Therefore, according to Eqs. (10) and (15), the effective saturation curve S_e can be computed by:

$$S_e = \frac{\int_{R_{min}}^{R_h} V_p(R) dN}{\int_{R_{min}}^{R_{max}} V_p(R) dN} = \frac{R_h^{2-D} - R_{min}^{2-D}}{R_{max}^{2-D} - R_{min}^{2-D}}. \quad (19)$$

Using the same hypothesis and neglecting film flow on capillary surfaces, we can obtain the relative permeability curve. The main contribution to the volumetric flow through the REV q (m³/s) can be computed by integrating the individual volumetric flow rates over the pores that remain fully saturated ($R_{min} \leq R \leq R_h$):

$$q = \int_{R_{min}}^{R_h} \bar{v}(R) \pi R^2 dN = \frac{\rho_w g}{8\eta_w \tau} \frac{\Delta h}{L} \frac{\pi D R_{REV}^D}{4-D} (R_h^{4-D} - R_{min}^{4-D}). \quad (20)$$

Otherwise, according to Buckingham-Darcy's law (1907), the total volumetric flow rate through the REV can be expressed as:

$$q = \frac{\rho_w g}{\eta_w} k k_{rel} \frac{\Delta h}{L} \pi R_{REV}^2. \quad (21)$$

Combining Eqs. (20) and (21) we can define analytical expressions for permeability and relative permeability:

$$k = \frac{D}{8\tau(4-D)R_{REV}^{2-D}} (R_{max}^{4-D} - R_{min}^{4-D}), \quad (22)$$

and

$$k_{rel}(R_h) = \frac{R_h^{4-D} - R_{min}^{4-D}}{R_{max}^{4-D} - R_{min}^{4-D}}. \quad (23)$$

Relative permeability k_{rel} can also be expressed in terms of effective saturation S_e . By combining Eqs. (19) and (23) we obtain the following equation:

$$k_{rel} = \frac{[S_e (1 - \alpha^{2-D}) + \alpha^{2-D}]^{\frac{4-D}{2-D}} - \alpha^{4-D}}{1 - \alpha^{4-D}}, \quad (24)$$

where

$$\alpha = \frac{R_{min}}{R_{max}}. \quad (25)$$

Note that the parameter α can be used as a measurement of the soil gradation. High values of α can be associated to well graded soils while low values to poorly graded soils. Then, for $R_{max} \gg R_{min}$ ($\alpha \rightarrow 0$), Eq. (24) can be reduced to:

$$k_{rel}(S_e) = S_e^{\frac{4-D}{2-D}}. \quad (26)$$

It can be observed that this expression is similar to the power law of the well-known Brooks and Corey model (1964).

2.2.2 Electrokinetic properties

The electrokinetic phenomenon is a coupling between hydraulic and electrical processes in a medium. Based on the previous description of macroscopic hydraulic properties we compute the effective excess charge density \hat{Q}_v^{REV} carried by the water flow in the REV. We consider similar conditions of saturation as in Section 2.2.1: the REV is initially fully saturated and a pressure head h is applied, drying the larger pores. Therefore, only the capillaries that remain fully saturated ($R_{min} \leq R \leq R_h$) contribute to the effective excess charge density \hat{Q}_v^{REV} (C/m³) that can be computed by:

$$\hat{Q}_v^{REV} = \frac{1}{v_D \pi R_{REV}^2} \int_{R_{min}}^{R_h} \hat{Q}_v^R \bar{v}(R) \pi R^2 dN, \quad (27)$$

where $v_D = \frac{\rho_w g}{\eta_w} k_{rel} k \frac{\Delta h}{L}$ (m/s) is the Darcy's flow. Substituting Eqs. (11), (13) and (15) in Eq. (27) yields:

$$\hat{Q}_v^{REV} = 8N_A e_0 C_w l_D^2 \left[-\frac{2e_0 \zeta}{k_B T} - \left(\frac{e_0 \zeta}{3k_B T} \right)^3 \right] \frac{\rho_w g}{8\eta_w \tau} \frac{\Delta h}{L} \frac{D}{v_D R_{REV}^{2-D} (2-D)} [R_h^{2-D} - R_{min}^{2-D}]. \quad (28)$$

Finally, combining Eqs. (16), (19) and (28) we obtain the following expression for \hat{Q}_v^{REV} :

$$\hat{Q}_v^{REV}(S_e, C_w^0) = N_A e_0 C_w^0 \left[-\frac{2e_0 \zeta}{k_B T} - \left(\frac{e_0 \zeta}{3k_B T} \right)^3 \right] \left(\frac{l_D}{\tau} \right)^2 \frac{\phi}{k} \frac{S_e}{k_{rel}(S_e)}. \quad (29)$$

This equation is the main contribution of this paper as it describes the entire model to determine the effective excess charge density in a porous medium under partially saturated conditions derived from geometrical properties and physical laws. This closed-form

expression relies on two kind of medium properties: (1) petrophysical properties, i.e., permeability, porosity, effective saturation and hydraulic tortuosity, and (2) electro-chemical properties, i.e., ionic concentration, zeta potential, and Debye length.

Note that under saturated conditions (i.e., $S_e = 1$), Eq. (29) is equivalent to the model of Guarracino and Jougnot [2018]. Then, \hat{Q}_v^{REV} can be expressed as the product between the effective excess charge density for saturated conditions $\hat{Q}_v^{REV,sat}$ (C/m³) and the relative effective excess charge density $\hat{Q}_v^{REV,rel}$ [dimensionless, see Jougnot et al., 2015]:

$$\hat{Q}_v^{REV} = \hat{Q}_v^{REV,sat} \hat{Q}_v^{REV,rel}(S_e) \quad (30)$$

where

$$\hat{Q}_v^{REV,rel}(S_e) = \frac{S_e}{k_{rel}(S_e)}. \quad (31)$$

It can be seen that the relative effective excess charge density defined by Eq. (31) depends only on hydraulic variables. By considering the proposed relationship between k_{rel} and S_e (Eq. (24)), the following analytical expression of Eq. (31) can be obtained:

$$\hat{Q}_v^{REV,rel}(S_e) = \frac{S_e(\alpha^{D-4} - 1)}{[S_e(\alpha^{D-2} - 1) + 1]^{\frac{4-D}{2-D}} - 1}. \quad (32)$$

The above equation depends on the model parameters D and α , to test their role on $\hat{Q}_v^{REV,rel}$ estimates, we perform a parametric analysis. Figure 2 shows $\log(\hat{Q}_v^{REV,rel})$ values for the following ranges of variability of each parameter: $1 < D < 2$ and $10^{-6} < \alpha < 10^{-1}$ while we considered as reference values $D = 1.6$ and $\alpha = 10^{-3}$. Figure 2a shows that the relative effective excess charge density $\hat{Q}_v^{REV,rel}$ decreases faster when effective saturation decreases for low fractal dimension values which are associated to coarse textured soils. Figure 2b shows that for low values of parameter α (e.g. well graded soils), $\hat{Q}_v^{REV,rel}$ decreases faster and its values change in 10 orders of magnitude. By comparing both panels, it can be noticed that $\hat{Q}_v^{REV,rel}$ is greater than 1 and may vary several orders of magnitude. Indeed, variations of parameter α produce the more significant effect in $\hat{Q}_v^{REV,rel}$ values.

A similar expression for the relative effective excess charge density was obtained by Jackson [2010] based on the coupling coefficient approach to estimate the streaming currents in a bundle of capillary tubes (see more details in Sec. 4). Nevertheless, it is important to remark that the proposed model provides an analytical closed-form expression (Eq. (29)) to estimate the total effective excess charge density \hat{Q}_v^{REV} .

Assuming that $R_{min} \ll R_{max}$, Eq. (32) can be expressed as:

$$\hat{Q}_v^{REV,rel}(S_e) = \frac{1}{S_e^a}. \quad (33)$$

where $a = 2/(2 - D)$. Note that $\hat{Q}_v^{REV,rel}$ depends inversely on effective saturation with exponent $a > 2$. Linde et al. [2007] proposed a volume averaging model to estimate $\hat{Q}_v^{REV,rel}$ as a function of water saturation which considers $a = 1$ (more details in Sec. 4). However, this model has been shown to underestimate the effective excess charge when compared to flux averaging approaches [e.g., Jougnot et al., 2012].

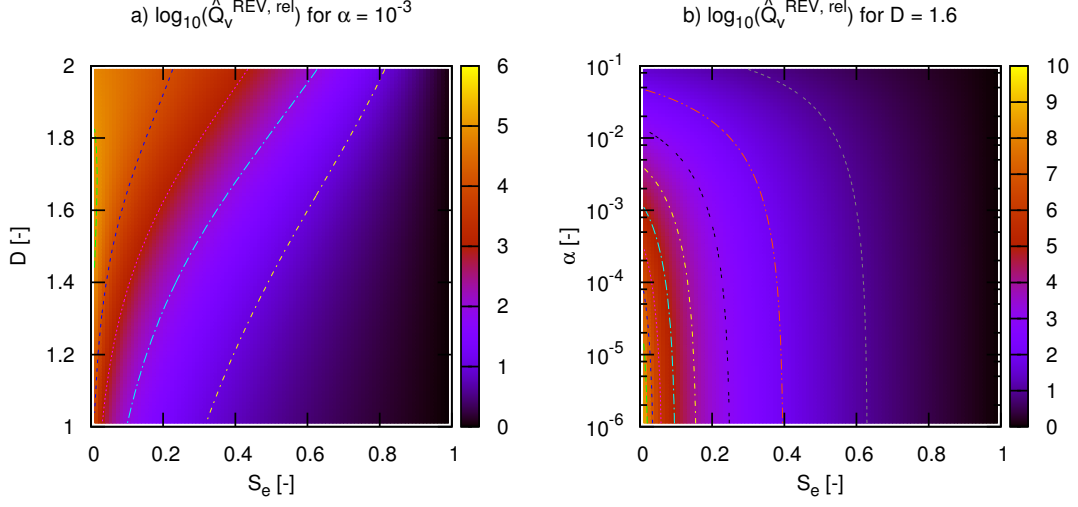


Figure 2: Parametric analysis of relative effective excess charge density $\hat{Q}_v^{REV,rel}$ as a function of effective saturation S_e : a) sensitivity to fractal dimension D for a reference value of α , and b) sensitivity to α for a reference value of D

2.3 Relationship between \hat{Q}_v^{REV} and permeability

In this section, we derive an expression to estimate the effective excess charge density \hat{Q}_v^{REV} from permeability under unsaturated conditions. Assuming that $R_{min} \ll R_{max}$, a relationship between the petrophysical properties of the medium ϕ and k can be obtained by combining Eqs. (16) and (22):

$$\phi = \left(\frac{k}{\gamma} \right)^{\frac{2-D}{4-D}}, \quad (34)$$

where $\gamma = \frac{DR_{REV}^2}{8\tau(4-D)} \left(\frac{2-D}{\tau D} \right)^{\frac{4-D}{2-D}}$. Replacing this expression in Eq.(29) and taking logarithm on both sides of the resulting equation, it yields

$$\log_{10} \left(\hat{Q}_v^{REV} \right) = A + B \log_{10}(k k_{rel}), \quad (35)$$

where

$$A = \log_{10} \left\{ \frac{N_A e_0 C_w^0}{\gamma^{\frac{2-D}{4-D}}} \left[-\frac{2e_0 \zeta}{k_B T} - \left(\frac{e_0 \zeta}{3k_B T} \right)^3 \right] \left(\frac{l_D}{\tau} \right)^2 \right\}, \quad (36)$$

and

$$B = -\frac{2}{4-D}. \quad (37)$$

Note that the constant A depends on chemical and hydraulic parameters, while constant B depends only on the fractal dimension. One can remark that under saturated conditions,

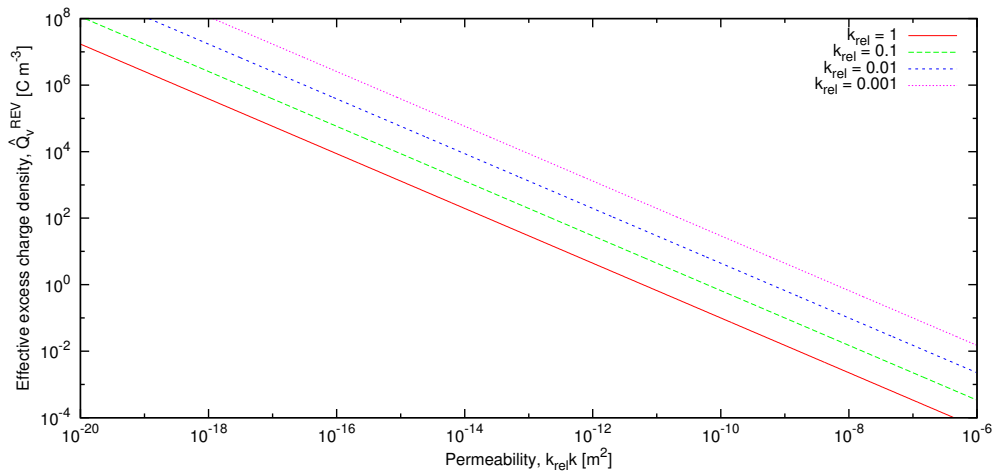


Figure 3: Effective excess charge density as a function of the product between the relative and intrinsic permeabilities. The red solid line represents the empirical relationship for saturated conditions of Jardani et al. [2007].

$k_{rel} = 1$, Eq. (35) is equivalent to the empirical relationship proposed by Jardani et al. [2007] where $A = -9.2349$ and $B = -0.8219$. These constant values were obtained by fitting the $\log(\hat{Q}_v^{REV,sat}) - \log(k)$ relationship to a large set of experimental data including different lithologies and salinities. This empirical relationship has been successfully used in several studies to directly estimate $\hat{Q}_v^{REV,sat}$ values from permeability [e.g., Revil and Mahardika, 2013, Jardani and Revil, 2009, Jougnot et al., 2013, Roubinet et al., 2016]. Besides, Eq. (35) represents the extension to partially saturated media of the recent analytical expression derived by Guarracino and Jougnot [2018] which provides a theoretical justification to the relationship of Jardani et al. [2007].

Figure 3 shows the effective excess charge density \hat{Q}_v^{REV} as a function of permeability for different k_{rel} values. The empirical relationship proposed by Jardani et al. [2007] is also shown in the Figure. Note that while the slope of the curves remains unchanged, the resulting estimates of \hat{Q}_v^{REV} are displaced to higher values when k_{rel} decreases.

3 Application of the model to different hydrodynamic properties

In this section, we analyze the effect of soil texture and permeability models on the estimates of the relative effective excess charge density.

3.1 Estimation of $\hat{Q}_v^{REV,rel}$ for different soil textures

The relative effective excess charge density depends only on the hydraulic properties of the medium, S_e and k_{rel} . Hence, to study the effect of soil textures on $\hat{Q}_v^{REV,rel}$, we consider that the proposed permeability model is related to soil textures through the fractal dimension D . Given the similarity between the proposed and Brooks and Corey (1964) models, we compare both $S_e(h)$ expressions to obtain a relationship between their

parameters. Therefore, the performance of Eq. (33) to estimate $\hat{Q}_v^{REV,rel}$ can be analyzed using typical values of Brooks and Corey parameters for 11 soil textures from Brakensiek and Rawls [1992] (see Table 1). Assuming $R_{max} \gg R_{min}$, Eq. (19) can be expressed as:

$$S_e = \left(\frac{R_h}{R_{max}} \right)^{2-D} = \left(\frac{h_{min}}{h} \right)^{2-D} \quad (38)$$

where h_{min} is obtained using Eq. (18).

The water retention equation proposed by Brooks and Corey model (1964) is given by:

$$S_e = \left(\frac{h_b}{h} \right)^\lambda \quad (39)$$

where λ is the pore-size distribution index and h_b the so called bubbling pressure head. Comparing Eqs. (38) and (39), the model parameters can be related through $D = 2 - \lambda$ and $R_{max} = \frac{2T_s}{\rho_w g h_b}$ where the contact angle β is assumed to be zero [Bear, 1998]. Table 1 lists the resulting parameters for all the soil textures.

In Figure 4 values of k_{rel} and $\hat{Q}_v^{REV,rel}$ are presented as a function of S_e assuming a ionic concentration of 1×10^{-3} mol/L. The effective saturation values are limited to the values predicted by Eq. (38) within the range $5l_D \leq R \leq R_{max}$, that is the radius range where the electrical double layer from the pore walls do not overlap and Eq. (13) is valid [Guarracino and Jougnot, 2018]. It is interesting to observe that for a fixed saturation value, the finest soil textures produce the higher values of $\hat{Q}_v^{REV,rel}$ (e.g. for $S_e = 0.6$, the $\hat{Q}_v^{REV,rel}$ values for sand and clay differ in 3 orders of magnitude). Also note that the maximum values of relative effective excess charge density are in the range of $10^6 - 10^7$ for all the soil textures being the higher values associated to fine soil textures at high S_e values.

3.2 Estimation of $\hat{Q}_v^{REV,rel}$ using different constitutive models

In order to test the performance of k_{rel} models to estimate $\hat{Q}_v^{REV,rel}$, we fit predicted relative effective excess charge density values calculated as S_e/k_{rel} with van Genuchten [1980] and Brooks and Corey [1964] models, and the proposed $k_{rel}(S_e)$ relationship (Eq. (32)). For this analysis, we considered measured effective saturation-relative permeability data from Mualem [1976]. Then, an analytical expression for $\hat{Q}_v^{REV,rel}$ can be obtained for each relative permeability model:

$$\hat{Q}_v^{REV,rel} = \frac{S_e^{1/2}}{\left[1 - \left(1 - S_e^{1/m} \right)^m \right]^2}, \quad (40)$$

$$\hat{Q}_v^{REV,rel} = \frac{1}{S_e^{2+2/\lambda}}, \quad (41)$$

where m and λ are dimensionless empirical parameters related to the pore size distribution in the medium for the van Genuchten and Brooks and Corey models, respectively.

The parameters of the different k_{rel} models (m , λ , D and α) were fitted using an exhaustive search method and the root-mean-square deviation (RMSD) was calculated

Table 1: Brooks and Corey parameters from the water retention equation for different soil textures [Brakensiek and Rawls, 1992] and the corresponding values of the proposed model parameters

Texture	Brooks and Corey		Proposed model	
	$h_b[m]$	λ	$R_{max}[m]$	D
Sand	0.073	0.592	2.044×10^{-4}	1.408
Loamy sand	0.087	0.474	1.707×10^{-4}	1.526
Sandy loam	0.147	0.322	1.012×10^{-4}	1.678
Loam	0.112	0.220	1.329×10^{-4}	1.780
Silt loam	0.208	0.211	7.147×10^{-5}	1.789
Sandy clay loam	0.281	0.250	5.284×10^{-5}	1.750
Clay loam	0.259	0.194	5.731×10^{-5}	1.806
Silty clay loam	0.326	0.151	4.557×10^{-5}	1.849
Sandy clay	0.292	0.168	5.086×10^{-5}	1.832
Silty clay	0.342	0.127	4.339×10^{-5}	1.873
Clay	0.373	0.131	3.978×10^{-5}	1.869

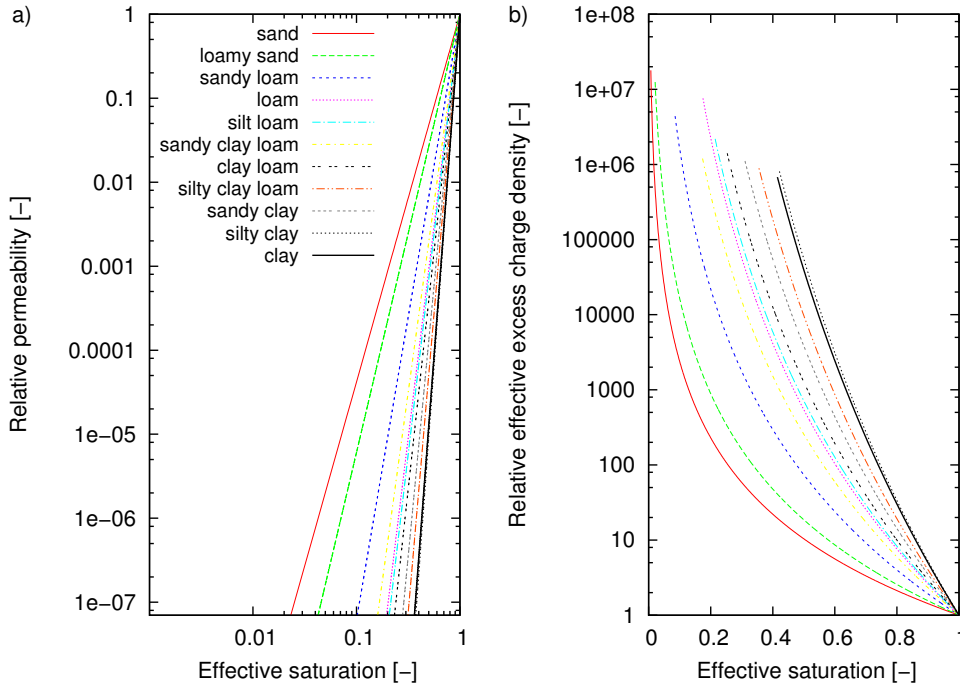


Figure 4: Analysis of the proposed model for different soil textures. a) The relative permeability is calculated using Eq. (26) and b) the relative effective excess charge density is estimated using Eq. (33)

Table 2: Values of the fitted parameters for van Genuchten (1980), Brooks and Corey (1964) and the proposed relative permeability model (Eq. (24)), and the corresponding RMSD

Soil type	van Genuchten		Brooks and Corey		Eq. (24)		
	m	RMSD	λ^{-1}	RMSD	D	α	RMSD
Sable de riviere	0.863	0.226	0	0.270	1.154	0.025	0.250
Rubicon sandy loam	0.802	0.086	0.186	0.171	1.597	0.057	0.086

taking logarithm differences due to the wide range of $\hat{Q}_v^{REV,rel}$ values. Table 2 lists the resulting parameter values and Figure 5 shows the comparison between the fit of Eqs. (32), (40) and (41) to two sets of experimental data (Rubicon sandy loam and Sable de riviere). It can be noticed that all the models produce good agreements with the predicted data. However, for Sable de riviere, parameter λ requires unrealistic values in order to fit $\hat{Q}_v^{REV,rel}$ data at low saturations.

4 Previous models

In this section, we review some recent models to describe SP signals generated under partially saturated conditions (see Table 3), based on both the coupling coefficient and the effective excess charge approaches.

4.1 Description of previous models

Wurmstich and Morgan [1994] estimated SP signals from the coupling coefficient approach when two-phase (air-water) flow occurs. They predicted that C_{EK} should increase with decreasing water saturation under the assumption that the nonwetting phase (air) is transported as bubbles. However, when both phases are homogeneously distributed throughout the pore space, this assumption is not valid. Perrier and Morat [2000] studied daily variations of electric potential data measured over several week which were interpreted as SP signal produced by unsaturated flow in the media. Based on the coupling coefficient approach, they inferred an empirical relationship to explain the dependence $C_{EK}(S_w)$ under the assumption that the electrical currents were affected by the unsaturated state similarly to the effect on the hydrological flow. Guichet et al. [2003] established from measured SP signals in a sand column during a drainage experiment that the coupling coefficient decreases linearly with decreasing effective water saturation. Darnet and Marquis [2004] performed synthetic 1D modeling of SP signals by estimating these signals from the coupling coefficient approach for air-water flow. They assumed that C_{EK} increases when water saturation decreases by considering that the air is transported as bubbles. Revil and Cerepi [2004] measured the coupling coefficient as a function of water saturation of two consolidated rock samples. To describe the dependence of $C_{EK}(S_w)$, they developed a petrophysical relationship which includes the effect of surface electrical conductivity.

Table 3: List of some of the previous models describing the electrokinetic phenomenon in SP signals derived from the coupling coefficient or excess charge approach

Reference	Coupling coefficient approach	Excess charge approach
Wurmstich and Morgan [1994] ⁽¹⁾	$C_{EK} = \frac{(1-w)C_v}{S_w^n}$	—
Perrier and Morat [2000]	$C_{EK} = \frac{C_{EK}^{sat} k_{rel}(S_w)}{S_w^n}$	—
Guichet et al. [2003]	$C_{EK} = C_{EK}^{sat} S_w$	—
Darnet and Marquis [2004]	$C_{EK} = \frac{\epsilon \zeta}{\eta_w \sigma S_e}$	—
Revil and Cerepi [2004] ⁽²⁾	$C_{EK} = C_{EK}^{sat} \frac{\beta_{(+)}(\sqrt{R^2+1}+R) + \beta_{(-)}(\sqrt{R^2+1}-R)}{\beta_{(+)}(\sqrt{R_S^2+1}+R_S) + \beta_{(-)}(\sqrt{R_S^2+1}-R_S)}$	
Linde et al. [2007] and Revil et al. [2007]	$C_{EK} = C_{EK}^{sat} \frac{k_{rel}(S_w)}{S_w \sigma_{rel}(S_w)}$	$\hat{Q}_v = \frac{\hat{Q}_v^{sat}}{S_w}$
Jackson [2010]	$C_{EK} = C_{EK}^{sat} \frac{S_e}{\sigma_{rel}(S_e)}$	$\hat{Q}_v = \frac{\hat{Q}_v^{sat} S_e}{k_{rel}(S_e)}$
Jougnot et al. [2012] ⁽³⁾	$C_{EK} = -\frac{\hat{Q}_v k}{\eta_w \sigma}$	$\hat{Q}_v = \frac{\int_{R_{min}}^{R_{Sw}} \hat{Q}_v^R(R, C_w^0) v^R(R) f_D(R) dR}{\int_{R_{min}}^{R_{Sw}} v^R(R) f_D(R) dR}$
Allègre et al. [2012] ⁽⁴⁾	$C_{EK} = C_{EK}^{sat} S_e [1 + \beta(1 - S_e)^\gamma]$	—
Zhang et al. [2017] ⁽⁵⁾	—	$\hat{Q}_v = \hat{Q}_v^{sat} (p S_e^{-q} + r)$

⁽¹⁾ C_v is coupling coefficient in the brine and w the hydrodynamic resistance factor

⁽²⁾ R is the quotient between the excess charge in the pore water and the brine concentration; β , the mobility of the ions and R_S , the quotient between R and S_e

⁽³⁾ f_D is the capillary size distribution function

⁽⁴⁾ β and γ are two fitting parameters

⁽⁵⁾ p , q and r are the model fitting parameters

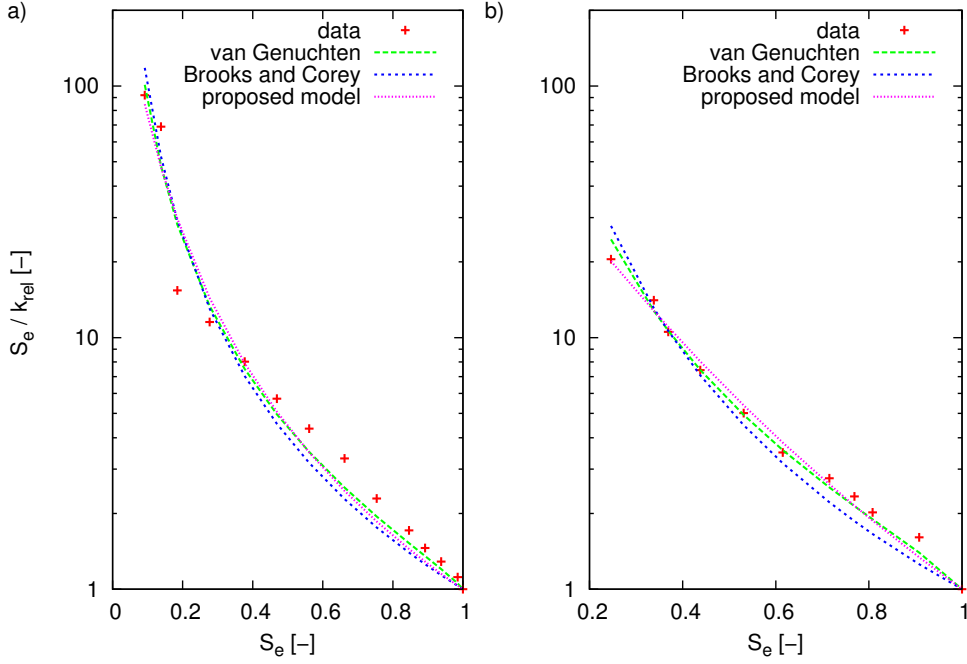


Figure 5: Analysis of $\hat{Q}_v^{REV,rel}$ for different k_{rel} models (van Genuchten, Brooks and Corey and Eq. (24)) for two soils: a) Sable de riviere and b) Rubicon sandy loam (data from Mualem [1976])

Based on a volume averaging approach, Linde et al. [2007] and Revil et al. [2007] considered that as the effective water saturation decreases in the pore volume (while the amount of surface charge remains constant), the relative effective excess charge density should increase in the pore water. Then, they proposed that the effective excess charge density \hat{Q}_v scales with the inverse of water saturation. Although this model has been shown to reproduce fairly well the behavior of the relative effective excess charge density in well-sorted media [e.g., Linde et al., 2007, Mboh et al., 2012, Jougnot and Linde, 2013], it does not seem appropriate for more heterogeneous media. As shown by Jougnot et al. [2012] and Jougnot et al. [2015], it seems to underestimate the increase of \hat{Q}_v with decreasing saturation.

Jackson [2010] proposed a capillary tube model to study the electrokinetic coupling during a two-phase flow (water-air). Under the hypotheses of a thin EDL and that the charge on the surface of each capillary is constant, he derived expressions for the coupling coefficient and the effective excess charge density by considering the streaming currents under partial and total saturated conditions. The relative factor of these expressions C_{EK}^{rel} and $\hat{Q}_v^{REV,rel}$ are expressed as functions of petrophysical properties. Note that the proposed model (Eq. (29)) is based on the effective excess charge dragged by the water flux and on the model to estimate \hat{Q}_v in a single pore proposed by Guarracino and Jougnot [2018]. Then, the $\hat{Q}_v^{REV,rel}$ expressions of both models are consistent although being derived from the two different approaches used to study the electrokinetic coupling. Nevertheless, the proposed model has a closed-form analytical expression which allows to estimate the total effective excess charge density from petrophysical parameters.

Following the works of Jackson [2008, 2010] and Linde [2009] and taking into account the heterogeneous nature of soils, Jougnot et al. [2012] proposed a capillary-based approach to represent the porous media. In their model, the capillary size distribution can be inferred from the hydrodynamic curves of the porous medium: the water retention (WR) and relative permeability (RP) curve. The equivalent pore size distribution can be derived from either of the two curves. The effective excess charge density is calculated by numerically integrating the distribution of the pore water flux and the distribution of excess charge density within the capillaries (i.e., the flux averaging approach).

Allègre et al. [2012] proposed an empirical relationship for the electrokinetic coupling coefficient inferred from drainage experiments performed within a column filled with a clean sand. This model predicts a non-monotonous behavior of the C_{EK} coefficient as a function of water saturation. Note that the model of Jougnot et al. [2012] also predicts a non-monotonous behavior of the coupling coefficient as a function of the water saturation depending on the porous medium. It is the case for Fontainebleau sand [i.e., the one used by Allègre et al., 2012] as it can be seen in Fig. 6c and 6d of Jougnot et al. [2012].

Recently, Zhang et al. [2017] proposed a power law function to model the relative effective excess charge density \hat{Q}_v^{rel} as a function of effective saturation for two sandstone core samples during drainage and imbibition experiments. This empirical model depends on three parameters p , q and r which are determined by curve fitting to the mean values of $\hat{Q}_v^{rel}(S_e)$ at each value of water saturation for a given sample and displacement. In addition, they placed a constraint on two of the model parameters ($p + r = 1$) since the relative effective excess charge density must equal 1 when the sample is fully saturated.

4.2 Quantitative comparison with \hat{Q}_v models

In this section, we compare the proposed model with the effective excess charge models proposed by Linde et al. [2007], Jougnot et al. [2012] and Zhang et al. [2017] described previously.

Firstly, Eq. (29) is compared with the models of Linde et al. [2007] and Jougnot et al. [2012]. Saturated effective excess charge values are required in order to estimate \hat{Q}_v^{REV} using the $\hat{Q}_v^{REV,rel}$ model of Linde et al. [2007]. Then, the empirical relationship of Jardani et al. [2007] was considered to predict $\hat{Q}_v^{REV,sat}$. In their work, Jougnot et al. [2012] obtained \hat{Q}_v^{REV} values for different soil textures from the WR and RP approaches using the hydrodynamic functions from van Genuchten [1980]. To ensure a consistent comparison, we also considered that constitutive model to estimate the permeability values in the proposed model. The parameters used for the different soil textures are listed in Table 4 [Carsel and Parrish, 1988]. Then, we considered that the soils are saturated with a NaCl electrolyte at $T = 20^\circ C$ with a concentration of 5×10^{-3} mol/L. Figure 6 shows the WR and RP models from the flux averaging of Jougnot et al. [2012], the volume average approach from Linde et al. [2007] and the proposed model Eq. (29). It can be seen that the proposed model shows an important increase of \hat{Q}_v^{REV} values when water saturation decreases which is consistent with the previous models. However, the proposed model predicts much larger values for low saturations. The difference between the models is of several orders of magnitude (1 - 6 orders), being the strongest differences between the WR approach and the proposed model. The model of Linde et al. [2007] also differs significantly from the proposed model and it seems to underestimate the increase of \hat{Q}_v^{REV}

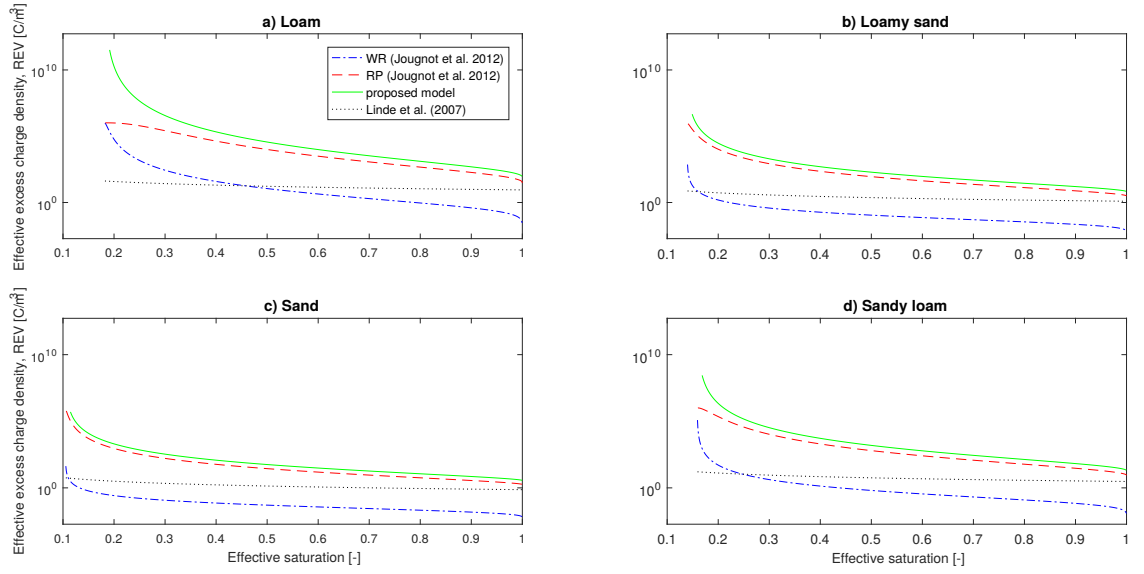


Figure 6: Comparison between the proposed model (Eq. (29)), the water retention (WR) and relative permeability (RP) approaches from Jougnot et al. [2012] and the model of Linde et al. [2007] for different soil textures: a) loam, b) loamy sand, c) sand and d) sandy loam

Table 4: Typical hydrodynamic values for the van Genuchten-Mualem model as proposed by Carsel and Parrish [1988]

Texture	ϕ	S_w^r	m	$K(m/s)$
Loam	0.43	0.034	0.360	2.89×10^{-6}
Loamy sand	0.41	0.023	0.561	4.05×10^{-5}
Sand	0.43	0.019	0.627	8.25×10^{-5}
Sandy loam	0.41	0.027	0.471	1.23×10^{-5}

with decreasing saturation. Nonetheless, it can be noticed that the RP approach produces the smallest differences with the proposed model.

Finally, the relative effective excess charge density model (Eq. (32)) is compared with the empirical model of Zhang et al. [2017]. Figure 7 shows $\hat{Q}_v^{REV,rel}$ as a function of effective saturation for two sandstones (Stainton and St. Bees) during drainage and imbibition experiments. The fitted parameters were $D = 1.223$ and $\alpha = 4.995 \times 10^{-8}$ for drainage, and $D = 1.01$ and $\alpha = 0.020$ for imbibition. We did not expect an exact fit of the models since they differ. However, both models are able to predict that the relative effective excess charge density strongly increases monotonically when water saturation decreases.

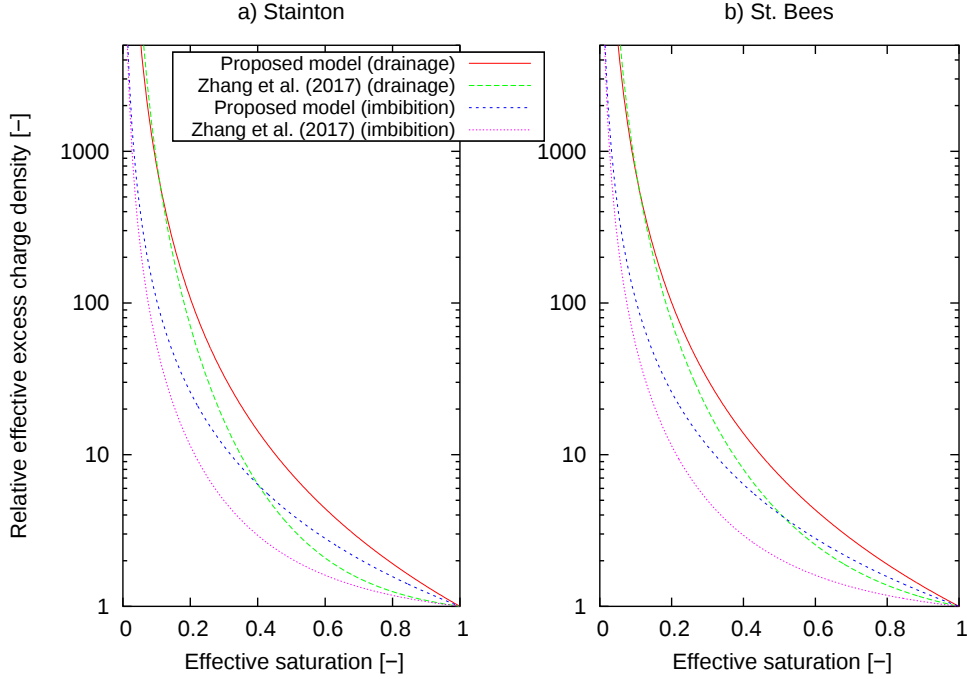


Figure 7: Comparison between the relative effective excess charge density model (Eq. (32)) and the empirical model proposed by Zhang et al. [2017] for two sandstones: a) Stainton and b) St. Bees, during drainage and imbibition experiments

5 Comparison with experimental data

In the present section, we test the proposed model against available experimental data from the research literature. These data sets consist of measured effective excess charge density-saturation or relative coupling coefficient-saturation values for different soil textures.

5.1 Laboratory data

The proposed relative effective excess charge density model is tested with laboratory data obtained by Revil and Cerepi [2004] and Cherubini et al. [2018]. The data from Revil and Cerepi [2004] consist of two sets of relative coupling coefficient values for two dolomite core samples (named E3 and E39, diameter ~ 3.8 cm and length < 8 cm). It is worth mentioning that the $\hat{Q}_v^{REV,rel}$ data values used to test our model were obtained from the C_{EK}^{rel} measured values using the following relationship between them [Revil and Leroy, 2004, Revil et al., 2007]:

$$\hat{Q}_v^{REV,rel} = \frac{C_{EK}^{rel} \sigma^{rel}}{k_{rel}}, \quad (42)$$

where the relative electrical conductivity σ^{rel} was estimated using Archie's second law (1942) $\sigma^{rel} = \sigma(S_w)/\sigma^{sat} = S^n$, being n the saturation index. The relative permeability k_{rel} was calculated using Brooks and Corey model since Revil and Cerepi [2004] fitted

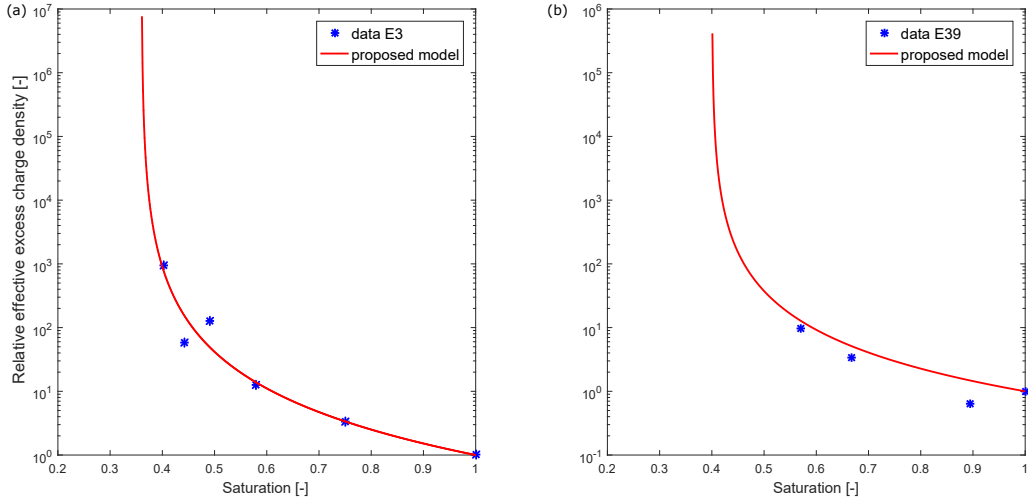


Figure 8: Relative effective excess charge density as a function of saturation for data sets from two dolomites samples from Revil and Cerepi [2004]

Table 5: Values of the hydraulic and electrical parameters used for the Brooks and Corey model (1964) and for Archie’s second law (1942)

Sample	Electrical parameter	Hydrological parameters	
	n	S_w^r	λ
E3	2.70	0.36	0.87
E39	3.48	0.40	1.65

this model parameters to their experimental results. Table 5 lists the parameters used to estimate these electrical and hydraulic properties of the two samples [Revil and Cerepi, 2004]. In order to provide a consistent comparison with the experimental data, $\hat{Q}_v^{REV,rel}$ values are estimated using Eq. (33).

Figure 8 shows the fit of Eq. (33) to predicted relative effective excess charge density values for the two dolomite samples. Parameter D of the proposed model is fitted by an exhaustive search method and the best agreement between the predicted values and the model is obtained for $D = 1.185$ ($RMSD = 0.567$) and $D = 1.002$ ($RMSD = 0.482$), for E3 and E39 respectively. It can be seen that for both data sets, the proposed model fits fairly well for all the range of saturation values.

The data from Cherubini et al. [2018] consist on three sets of effective excess charge density values for three carbonate core samples (named ESTA2, BRAU2 and RFF2, diameter 3.9cm and length 8cm). In this case, the $\hat{Q}_v^{REV,rel}$ data values were obtained by normalizing the \hat{Q}_v^{REV} data by the $\hat{Q}_v^{REV,sat}$ factor. Figure 9 shows the fit of Eq. (32) for the three carbonate samples and the model of Linde et al. [2007] is also shown. The best fitted parameters are listed in Table 6 which were found using the same method as for the previous laboratory data. It can be noted that Eq. (32) produces a fairly good agreement with the data sets for all the samples.

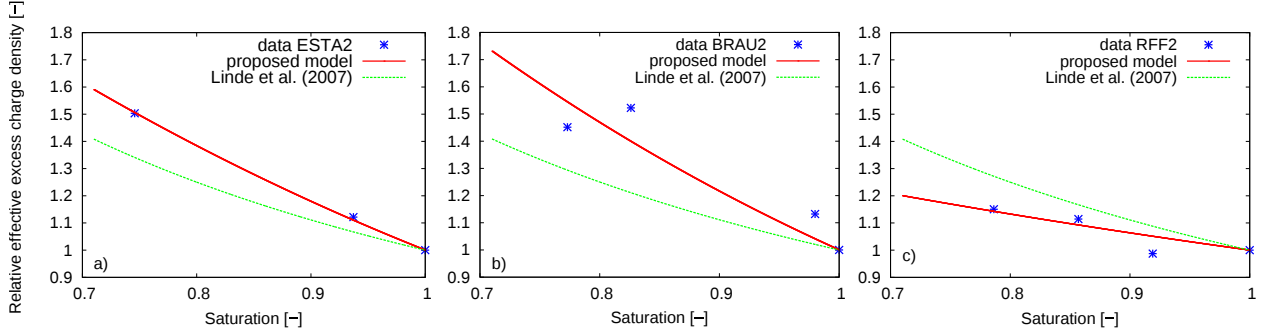


Figure 9: Relative effective excess charge density as a function of saturation for data sets from three carbonate samples from Cherubini et al. [2018].

Table 6: Values of the fitted parameters for Eq. (32) for the data sets from Cherubini et al. [2018]

Sample	S_w^{r*}	α	D	RMSD
ESTA2	0.31	0.407	1.999	6.913×10^{-3}
BRAU2	0.30	0.351	1.999	8.965×10^{-2}
RFF2	0.35	0.684	1.010	3.387×10^{-2}

* Values taken from Cherubini et al. [2018]

5.2 Field data

We now test our model in a larger scale with experimental data acquired by Doussan et al. [2002]. The experimental site consist of a lysimeter of about 9 m² surface area and 2 m depth packed with a sandy loam soil located in Avignon (France) in the experimental fields of the French National Institute for Agricultural Research (INRA). Following the analysis from Jougnot et al. [2012] on the lysimeter test from Doussan, we compare our model to the SP signals during 5 rainfall events. We converted the SP signals in \hat{Q}_v^{REV} values using a 1D hypothesis and the process explained in Jougnot et al. [2012]. As a result of the infiltration and evaporation of the rainwater, the water electrical conductivity σ_w was changing with time between 0.06 S/m and 0.20 S/m. From this parameter data measured during the experiment and the use of the empirical formula of Sen and Goode [1992], we obtained the ionic concentration C_w^0 of the free electrolyte that corresponds to each water electrical conductivity value (see Table 7). We then estimated the effective excess charge density using Eq. (33) to predict $\hat{Q}_v^{REV,rel}$ values. For $\hat{Q}_v^{REV,sat}$, we considered $\phi = 0.44$ [Doussan et al., 2002] and $\tau = 1.4$ as a representative value for the medium's tortuosity. This last parameter was estimated using the model of Winsauer et al. [1952] to determine the hydraulic tortuosity as [see the discussion in Guarracino and Jougnot, 2018]:

$$\tau = \sqrt{F\phi} \quad (43)$$

where F is the formation factor, we considered $F = 4.54$ from Doussan et al. [2002].

Figure 10 shows the different rainfall events fitted with the proposed model for three different C_w^0 values corresponding to the maximum, minimum and medium values of σ_w .

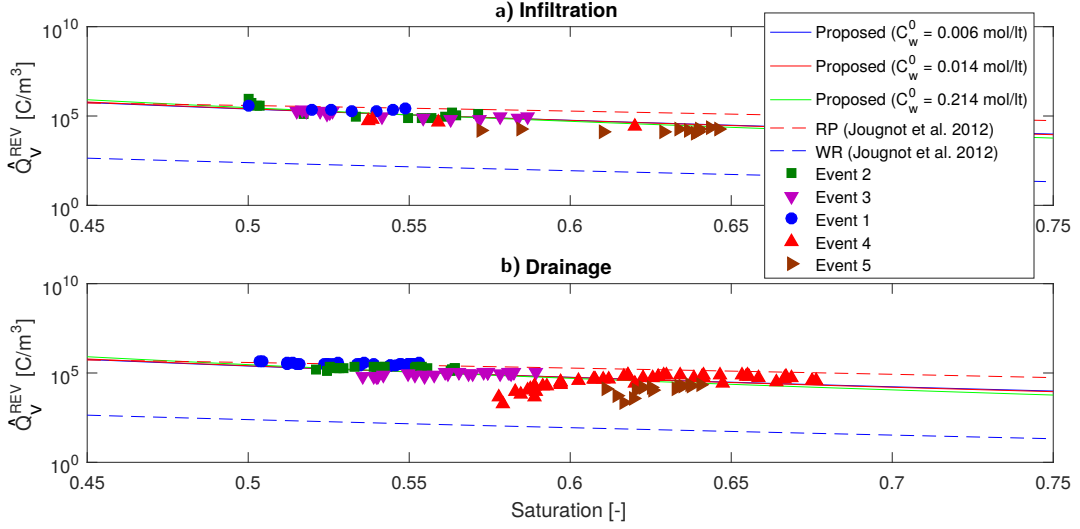


Figure 10: Effective excess charge density as a function of saturation during the five rainfall events considering infiltration and drainage phases. The solid lines represent the proposed model for different values of ionic concentration C_w^0 . The dashed lines represents the WR and RP approaches of Jougnot et al. [2012]

Table 7: Values of the fitted parameter D for the different values of water conductivity

σ_w (S/m)	C_w^0 (mol/L)	D	$RMSD$
0.06	0.006	1.749	3.219
0.13	0.014	1.758	3.188
0.20	0.214	1.793	3.056

Table 7 lists the resulting parameter D for each C_w^0 . Figure 10 also shows the approaches of Jougnot et al. [2012] and it can be observed that the proposed model fits well all the events and provides much more better results than the WR approach. Moreover, it also produces better predictions of \hat{Q}_v^{REV} values than the RP approach.

6 Discussion and conclusions

A physically based model for estimating the effective excess charge density under partially saturated conditions has been developed in the present study. The model was derived assuming that the porous media is represented by a bundle of tortuous capillary tubes with a fractal pore-size distribution and filled by a binary symmetric 1:1 electrolyte. Hydraulic and electrokinetic properties of the porous media were first estimated for a single pore at microscale and then upscaled to a REV assuming that a pore can be fully water saturated or completely dry. The resulting expression of \hat{Q}_v^{REV} is a function of water effective saturation and relative permeability, and has an analytical closed-form that depends on chemical parameters of the pore water (C_w^0 , l_D , ζ) and hydraulic parameters (τ , ϕ , k). The proposed model is the extension of the model derived by Guarracino and Jougnot [2018]

for saturated conditions. Therefore, our results show that estimates of the effective excess charge density can be easily extrapolated from saturated porous media to partially saturated conditions by introducing a $\hat{Q}_v^{REV,rel}$ factor which depends on the effective saturation and relative permeability of the media. It should be noted that the resulting expression of $\hat{Q}_v^{REV,rel}$ (Eq. (31)) is found consistent with the expression proposed by Jackson [2010] based on the framework of the coupling coefficient approach. In addition, the proposed model provides a relationship between \hat{Q}_v^{REV} and k_{rel} (Eq. (35)) which is similar to the empirical relationship of Jardani et al. [2007]. This effective excess charge density-permeability relationship extend to partially saturated conditions the recent analytical expression derived by Guarracino and Jougnot [2018] under saturated conditions.

The proposed relative effective excess charge density model depends only on the hydraulic properties of the media. The analysis on different soil textures showed significant differences in the $\hat{Q}_v^{REV,rel}$ values (Fig. 4). Indeed, it could be observed that for a given value of effective saturation, the maximum values of $\hat{Q}_v^{REV,rel}$ are associated to fined soil textures. The performance of $\hat{Q}_v^{REV,rel}$ was also tested when different constitutive models are used to predict relative permeability. The comparison between van Genuchten, Brooks and Corey and the proposed relative permeability (Eq. (24)) models showed that all of them can provide good estimates of $\hat{Q}_v^{REV,rel}$ values (Fig. 5).

The proposed model represents an improvement to predict \hat{Q}_v^{REV} values over the previous models of Linde et al. [2007] and Jougnot et al. [2012] also derived from the effective excess charge approach. When compared to the model of Jougnot et al. [2012], the proposed model produces a better match to the relative permeability approach rather than to the water retention (Fig. 6). The comparison of the proposed $\hat{Q}_v^{REV,rel}$ model against the empirical relationship proposed by Zhang et al. [2017] showed that both models predict the behavior of increasing $\hat{Q}_v^{REV,rel}$ when effective saturation decreases, although we did not expect a perfect match since the strong differences between the models.

The proposed \hat{Q}_v^{REV} and $\hat{Q}_v^{REV,rel}$ models were validated using experimental laboratory and field data, respectively. In both cases, the models were able to satisfactorily predict the magnitude of the data (Fig. 8, 9 and 10). Indeed, in the case of the field data, the \hat{Q}_v^{REV} model showed better agreement than the water retention and relative permeability approaches from Jougnot et al. [2012].

This study allowed the development of a new model to describe SP signals from the framework of the effective excess charge. This relationship is a explicit function of effective saturation while also depending on petrophysical parameters of the porous media. The analytical closed-form expression of this new model is easy to evaluate and its numerical implementation is straightforward. These observations may have practical implications for opening up to the use of the SP method to study physical phenomena occurring in the unsaturated zone such as infiltration [e.g., Jougnot et al., 2015], evaporation, CO₂ flooding [e.g., Büsing et al., 2017], or even contaminant fluxes [e.g., Linde and Revil, 2007].

References

- V. Allègre, F. Lehmann, P. Ackerer, L. Jouniaux, and P. Silliac. A 1-d modelling of streaming potential dependence on water content during drainage experiment in sand. *Geophysical Journal International*, 189(1):285–295, 2012.
- V. Allègre, L. Jouniaux, F. Lehmann, P. Silliac, and R. Toussaint. Influence of water pressure dynamics and fluid flow on the streaming-potential response for unsaturated conditions. *Geophysical Prospecting*, 63(3):694–712, 2015.
- G. E. Archie. The electrical resistivity log as an aid in determining some reservoir characteristics. *Transactions of the AIME*, 146(01):54–62, 1942.
- J. Bear. *Dynamics of fluids in porous media*. Dover Publications Inc., 1998.
- D. Brakensiek and W. Rawls. Comment on fractal processes in soil water retention by scott w. tyler and stephen w. wheatcraft. *Water resources research*, 28(2):601–602, 1992.
- R. H. Brooks and A. T. Corey. Hydraulic properties of porous media and their relation to drainage design. *Transactions of the ASAE*, 7(1):26–0028, 1964.
- E. Buckingham. Studies on the movement of soil moisture. *US Dept. Agric. Bur. Soils Bull.*, 38, 1907.
- H. Büsing, C. Vogt, A. Ebigbo, and N. Klitzsch. Numerical study on co2 leakage detection using electrical streaming potential data. *Water Resources Research*, 53(1):455–469, 2017.
- R. F. Carsel and R. S. Parrish. Developing joint probability distributions of soil water retention characteristics. *Water Resources Research*, 24(5):755–769, 1988.
- A. Cherubini, B. Garcia, A. Cerepi, and A. Revil. Streaming potential coupling coefficient and transport properties of unsaturated carbonate rocks. *Vadose Zone Journal*, 2018. doi: 10.2136/vzj2018.02.0030.
- R. F. Corwin and D. B. Hoover. The self-potential method in geothermal exploration. *Geophysics*, 44(2):226–245, 1979.
- H. P. G. Darcy. *Les Fontaines publiques de la ville de Dijon. Exposition et application des principes à suivre et des formules à employer dans les questions de distribution d’eau, etc.* 1856.
- M. Darnet and G. Marquis. Modelling streaming potential (sp) signals induced by water movement in the vadose zone. *Journal of hydrology*, 285(1):114–124, 2004.
- C. Doussan, L. Jouniaux, and J.-L. Thony. Variations of self-potential and unsaturated water flow with time in sandy loam and clay loam soils. *Journal of Hydrology*, 267(3): 173–185, 2002.

- E.-A. Fiorentino, R. Toussaint, and L. Jouniaux. Two-phase lattice boltzmann modelling of streaming potentials: influence of the air-water interface on the electrokinetic coupling. *Geophysical Journal International*, page ggw417, 2016.
- B. Ghanbarian-Alavijeh, H. Millán, and G. Huang. A review of fractal, prefractal and pore-solid-fractal models for parameterizing the soil water retention curve. *Canadian Journal of Soil Science*, 91(1):1–14, 2011.
- L. Guarracino and D. Jougnot. A physically-based analytical model to describe effective excess charge for streaming potential generation in water saturated porous media. *Journal of Geophysical Research: Solid Earth*, 2018.
- L. Guarracino, T. Rötting, and J. Carrera. A fractal model to describe the evolution of multiphase flow properties during mineral dissolution. *Advances in water resources*, 67: 78–86, 2014.
- X. Guichet, L. Jouniaux, and J.-P. Pozzi. Streaming potential of a sand column in partial saturation conditions. *Journal of Geophysical Research: Solid Earth*, 108(B3), 2003.
- H. V. Helmholtz. Studien über electrische grenzsichten. *Annalen der Physik*, 243(7): 337–382, 1879.
- R. Hunter. Zeta potential in colloid science: Principles and applications. *New York, USA*, 1981.
- M. D. Jackson. Characterization of multiphase electrokinetic coupling using a bundle of capillary tubes model. *Journal of Geophysical Research: Solid Earth*, 113(B4), 2008.
- M. D. Jackson. Multiphase electrokinetic coupling: Insights into the impact of fluid and charge distribution at the pore scale from a bundle of capillary tubes model. *Journal of Geophysical Research: Solid Earth*, 115(B7), 2010.
- A. Jardani and A. Revil. Stochastic joint inversion of temperature and self-potential data. *Geophysical Journal International*, 179(1):640–654, 2009.
- A. Jardani, A. Revil, A. Bolève, A. Crespy, J.-P. Dupont, W. Barrash, and B. Malama. Tomography of the darcy velocity from self-potential measurements. *Geophysical Research Letters*, 34(24), 2007.
- D. Jougnot and N. Linde. Self-potentials in partially saturated media: the importance of explicit modeling of electrode effects. *Vadose Zone Journal*, 12(2), 2013.
- D. Jougnot, N. Linde, A. Revil, and C. Doussan. Derivation of soil-specific streaming potential electrical parameters from hydrodynamic characteristics of partially saturated soils. *Vadose Zone Journal*, 11(1):0–0, 2012.
- D. Jougnot, J. G. Rubino, M. R. Carbajal, N. Linde, and K. Holliger. Seismoelectric effects due to mesoscopic heterogeneities. *Geophysical Research Letters*, 40(10):2033–2037, 2013.

- D. Jougnot, N. Linde, E. B. Haarder, and M. C. Looms. Monitoring of saline tracer movement with vertically distributed self-potential measurements at the hobe agricultural test site, vouldund, denmark. *Journal of Hydrology*, 521:314–327, 2015.
- J. Jurin. An account of some experiments shown before the royal society; with an enquiry into the cause of the ascent and suspension of water in capillary tubes. by james jurin, md and r. soc. s. *Philosophical Transactions*, 30(351-363):739–747, 1717.
- V. V. Kormiltsev, A. N. Ratushnyak, and V. A. Shapiro. Three-dimensional modeling of electric and magnetic fields induced by the fluid flow movement in porous media. *Physics of the earth and planetary interiors*, 105(3-4):109–118, 1998.
- P. Leroy and A. Revil. A triple-layer model of the surface electrochemical properties of clay minerals. *Journal of Colloid and Interface Science*, 270(2):371–380, 2004.
- N. Linde. Comment on characterization of multiphase electrokinetic coupling using a bundle of capillary tubes model by mathew d. jackson. *Journal of Geophysical Research: Solid Earth*, 114(B6), 2009.
- N. Linde and A. Revil. Inverting self-potential data for redox potentials of contaminant plumes. *Geophysical Research Letters*, 34(14), 2007.
- N. Linde, D. Jougnot, A. Revil, S. Matthäi, T. Arora, D. Renard, and C. Doussan. Streaming current generation in two-phase flow conditions. *Geophysical Research Letters*, 34(3), 2007.
- N. Linde, J. Doetsch, D. Jougnot, O. Genoni, Y. Dürst, B. J. Minsley, T. Vogt, N. Pasquale, and J. Luster. Self-potential investigations of a gravel bar in a restored river corridor. *Hydrology and Earth System Sciences*, 15(3):729–742, 2011.
- C. Mboh, J. Huisman, E. Zimmermann, and H. Vereecken. Coupled hydrogeophysical inversion of streaming potential signals for unsaturated soil hydraulic properties. *Vadose Zone Journal*, 11(2), 2012.
- J. R. Moore, S. D. Glaser, H. F. Morrison, and G. M. Hoversten. The streaming potential of liquid carbon dioxide in berea sandstone. *Geophysical research letters*, 31(17), 2004.
- Y. Mualem. A catalogue of the hydraulic properties of unsaturated soils. 1976.
- F. Perrier and P. Morat. Characterization of electrical daily variations induced by capillary flow in the non-saturated zone. *Pure & Applied Geophysics*, 157(5):785, 2000.
- A. Revil and A. Cerepi. Streaming potentials in two-phase flow conditions. *Geophysical Research Letters*, 31(11), 2004.
- A. Revil and A. Jardani. *The self-potential method: Theory and applications in environmental geosciences*. Cambridge University Press, 2013.
- A. Revil and P. Leroy. Constitutive equations for ionic transport in porous shales. *Journal of Geophysical Research: Solid Earth*, 109(B3), 2004.

- A. Revil and H. Mahardika. Coupled hydromechanical and electromagnetic disturbances in unsaturated porous materials. *Water resources research*, 49(2):744–766, 2013.
- A. Revil, P. Pezard, and P. Glover. Streaming potential in porous media 1. theory of the zeta potential. *Journal of Geophysical Research*, 104(B9):20021–20031, 1999a. doi: 10.1029/1999JB900089.
- A. Revil, H. Schwaeger, L. Cathles, and P. Manhardt. Streaming potential in porous media: 2. theory and application to geothermal systems. *Journal of Geophysical Research: Solid Earth*, 104(B9):20033–20048, 1999b.
- A. Revil, N. Linde, A. Cerepi, D. Jougnot, S. Matthäi, and S. Finsterle. Electrokinetic coupling in unsaturated porous media. *Journal of colloid and interface science*, 313(1): 315–327, 2007.
- D. Roubinet, N. Linde, D. Jougnot, and J. Irving. Streaming potential modeling in fractured rock: Insights into the identification of hydraulically active fractures. *Geophysical Research Letters*, 43(10):4937–4944, 2016.
- J. Saunders, M. Jackson, and C. Pain. A new numerical model of electrokinetic potential response during hydrocarbon recovery. *Geophysical Research Letters*, 33(15), 2006.
- P. N. Sen and P. A. Goode. Influence of temperature on electrical conductivity on shaly sands. *Geophysics*, 57(1):89–96, 1992.
- W. R. Sill. Self-potential modeling from primary flows. *Geophysics*, 48(1):76–86, 1983.
- M. v. Smoluchowski. Contribution to the theory of electro-osmosis and related phenomena. *Bull Int Acad Sci Cracovie*, 3:184–199, 1903.
- M. Soldi, L. Guarracino, and D. Jougnot. A simple hysteretic constitutive model for unsaturated flow. *Transport in Porous Media*, 120(2):271–285, 2017.
- L. D. Thanh, P. Do, N. Nghia, and N. X. Ca. A fractal model for streaming potential coefficient in porous media. *Geophysical Prospecting*, 2017.
- C. Tournassat, Y. Chapron, P. Leroy, M. Bizi, and F. Boulahya. Comparison of molecular dynamics simulations with triple layer and modified gouy–chapman models in a 0.1 m nacl–montmorillonite system. *Journal of Colloid and Interface Science*, 339(2):533–541, 2009.
- S. W. Tyler and S. W. Wheatcraft. Fractal processes in soil water retention. *Water Resources Research*, 26(5):1047–1054, 1990.
- M. T. van Genuchten. A closed-form equation for predicting the hydraulic conductivity of unsaturated soils. *Soil science society of America journal*, 44(5):892–898, 1980.
- J. Vinogradov and M. Jackson. Multiphase streaming potential in sandstones saturated with gas/brine and oil/brine during drainage and imbibition. *Geophysical Research Letters*, 38(1), 2011.

- E. B. Voytek, H. R. Barnard, D. Jougnot, and K. Singha. Propagation of diel transpiration signals in the subsurface using the self-potential method. *Hydrological Processes*, under review.
- M. Waxman and L. Smits. Electrical conductivities in oil-bearing shaly sands. *Society of Petroleum Engineers Journal*, 8(02):107–122, 1968.
- W. O. Winsauer, H. Shearin Jr, P. Masson, and M. Williams. Resistivity of brine-saturated sands in relation to pore geometry. *AAPG bulletin*, 36(2):253–277, 1952.
- B. Wurmstich and F. D. Morgan. Modeling of streaming potential responses caused by oil well pumping. *Geophysics*, 59(1):46–56, 1994.
- P. Xu. A discussion on fractal models for transport physics of porous media. *Fractals*, 23(03):1530001, 2015.
- B. Yu, J. Li, Z. Li, and M. Zou. Permeabilities of unsaturated fractal porous media. *International journal of multiphase flow*, 29(10):1625–1642, 2003.
- J. Zhang, J. Vinogradov, E. Leinov, and M. Jackson. Streaming potential during drainage and imbibition. *Journal of Geophysical Research: Solid Earth*, 2017.